Time scales at quantum phase transitions in the Lipkin-Meshkov-Glick model

F. de los Santos
Departamento de Electromagnetismo y Física de la Materia and Instituto Carlos I de Física Teórica y Computacional, Universidad de Granada, Fuentenueva s/n, 18071 Granada, Spain

E. Romera
Departamento de Física Atómica, Molecular y Nuclear and Instituto Carlos I de Física Teórica y Computacional, Universidad de Granada, Fuentenueva s/n, 18071 Granada, Spain

O. Castaños
Instituto de Ciencias Nucleares, Universidad Nacional Autónoma de México, Apartado Postal 70-543, Distrito Federal 04510, Mexico
(Received 29 August 2014; published 13 April 2015)

We report on quantum revivals and classical periodicities of wave packets centered around the ground state within the Lipkin-Meshkov-Glick model. Special attention is paid to the behavior at first- and second-order phase transitions. In line with previous studies, we find that away from criticality, characteristic times exhibit smooth, nonsingular behavior, but upon approaching the transition points they diverge as power laws with associated critical exponents. Finite-size effects are studied and the observed phenomenology is discussed in the framework of the time-energy uncertainty relation.

DOI: 10.1103/PhysRevA.91.043409 PACS number(s): 42.50.Md, 67.85.De, 64.70.Tg, 05.30.Rt

I. INTRODUCTION

The wave packet evolution in quantum systems is dramatically different from the classical ones due to, among other things, its associated interference effects. A striking example is provided by the unexpected periodicities observed in the long-time evolution of wave packets: Under suitable conditions (which we shall discuss shortly), propagating wave packets initially oscillate with the same period as they would in the classical limit, but eventually spread out and collapse. At later times, wave packets regain their initial shape, behave quasiclassically again, and a new cycle commences. This rich nonclassical behavior is embodied in the system's spectrum E_n, through the time evolution of the eigenstates e^{-iE_nt} (in units such that $\hbar = 1$). More precisely, if the wave packet is tightly spread around a large central level n_0 and the distance between levels is small enough, it is then legitimate to Taylor-expand E_n about this value,

$$E_n = E_{n_0} + E'_{n_0}(n-n_0) + \frac{E''_{n_0}}{2}(n-n_0)^2 + \cdots , \quad (1)$$

and consequently it is straightforward to obtain

$$e^{-iE_nt} = \exp\left[-iE_{n_0}t - 2\pi i(n-n_0)\frac{t}{T_{\rm Cl}} - 2\pi i(n-n_0)^2\frac{t}{T_{\rm R}} + \cdots\right], \quad (2)$$

where we have defined $T_{\rm Cl} = 2\pi/|E'_{n_0}|$ and $T_{\rm R} = 4\pi/|E''_{n_0}|$. Now, each term in the above expansion defines a relevant time scale. The first one $-iE_{n_0}$ just generates an unobservable overall phase. (In relativistic quantum mechanics, however, when both positive and negative levels are populated, $T_{\rm ZB} = \pi/E_{n_0}$ provides the frequency of *Zitterbewegung* oscillations [1,2].) The second one provides the so-called classical period, that is, the time over which the wave packet exhibits classical features. Lastly, the third term defines the revival time scale, which is purely quantum in origin and corresponds to the time it takes for the wave packet to regain (approximately) its original shape. Here, we shall not be concerned with other time scales that can be defined through Eq. (1), for instance the super-revival time. Revivals have attracted a great deal of attention over recent decades and to date several skillful applications have been developed [3].

At a quantum phase transition, due to quantum fluctuations systems undergo abrupt changes of state when a parameter, say γ, is varied [4]. The transition between two quantum phases can be of different orders and in every case the energy spectrum $E(\gamma)$ becomes nonanalytic at that value of γ, in the thermodynamic limit, and consequently the temporal scales for the time evolution as described in Eq. (2) may become nonanalytic as well. In [5], we addressed this problem by investigating the implications for time development of wave packets of traversing a quantum phase transition. There, by analyzing two different models, namely, the vibron model for the bending of polyatomic molecules and the Dicke model for a quantum radiation field interacting with a system of two-level atoms, we found evidence of revival behavior for wave packets centered around energy levels as low as the ground state. Furthermore, away from criticality, revival and classical times displayed a smooth, nonsingular behavior that changed to power-law divergences upon approaching a quantum critical point. Here, we expand on this subject by studying the time evolution of wave packets within the Lipkin-Meshkov-Glick (LMG) model of interacting fermions [6]. This model exhibits shape phase transitions of different orders (first-, second-, and third-order; see below) [7]. We confirm the general picture described above and extend the analysis to first-order phase transitions. Finite-size effects are studied and our findings are discussed in the context of the time-energy uncertainty relation.

 ©2015 American Physical Society

II. THE LMG MODEL

The LMG model was originally designed to describe shape phase transitions in nuclei [6], but it has also been used to describe many-body systems in other fields of physics, such as quantum optics, Bose-Einstein condensates, or Josephson junctions [8–14]. Phase transitions in the LMG model have been studied by means of different methods (see [7,15–21]), including a recent characterization in terms of the zeros of the Husimi function [22]. The LMG model considers N interacting fermions occupying two N-fold degenerate levels, separated by an energy ϵ. In terms of quasispin operators, the standard form of its Hamiltonian reads [6]

$$H = \varepsilon J_z + \tfrac{1}{2}V(J_+^2 + J_-^2) + \tfrac{1}{2}W\,(J_+J_- + J_-J_+)\,, \qquad (3)$$

where the angular momentum operators take their usual meaning and are related to the creation and annihilation of fermions [6].

The transformation

$$\gamma_x \equiv \frac{2j-1}{\varepsilon}(W+V), \quad \gamma_y \equiv \frac{2j-1}{\varepsilon}(W-V) \qquad (4)$$

casts the LMG Hamiltonian in the form

$$H = \varepsilon J_z - \varepsilon\frac{\gamma_x+\gamma_y}{2(2j-1)}J_z^2 + \varepsilon\frac{\gamma_x+\gamma_y}{2(2j-1)}J^2 + \varepsilon\frac{\gamma_x-\gamma_y}{4(2j-1)}(J_+^2+J_-^2), \qquad (5)$$

which facilitates a semiclassical analysis. Dividing now by $\varepsilon/2$ and adding the irrelevant constant $-j^2/(2j-1)(\gamma_x+\gamma_y)$ leads to the final expression

$$H_C = \frac{j^2}{2j-1}(\gamma_x+\gamma_y) + 2J_z - \frac{\gamma_x+\gamma_y}{2j-1}J_z^2 + \frac{\gamma_x-\gamma_y}{2(2j-1)}(J_+^2+J_-^2). \qquad (6)$$

A classical analysis of the Hamiltonian Eq. (6) allows one to distinguish different regions in the parameter space γ_x-γ_y according to the nature of the transition points [7,22]: (a) the crossing of the straight line $\gamma_x = \gamma_y$ ($\gamma_x < -1$) yields a first-order transition; (b) second-order phase transitions take place when the straight lines $\gamma_x = -1$ and $\gamma_y = -1$ and the point $(\gamma_x,\gamma_y) = (-1,-1)$ are crossed; (c) the crossing of the point $(\gamma_x,\gamma_y) = (-1,-1)$ along the straight line $\gamma_x = -\gamma_y - 2$ yields a third-order phase transition. We shall consider trajectories of the type: $\gamma_y = -\gamma_x - b$. For $b < -2$, the model Hamiltonian exhibits first-order quantum phase transitions at the point $(\gamma_x,\gamma_y) = (-b/2,-b/2)$ while for $b > -2$ second-order quantum phase transitions are present at the points

$$(\gamma_x,\gamma_y) = \{(-b+1,-1)\,,(-1,1-b)\}.$$

As examples of the first- and second-order phase transitions we consider the values $b = 4$ and $b = 0$, respectively, as shown in Fig. 1.

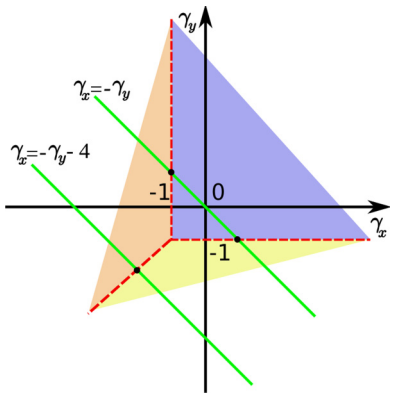

FIG. 1. (Color online) γ_x-γ_y phase diagram of the LMG model. The straight lines $\gamma_x = -\gamma_y$ and $\gamma_x = -\gamma_y - 4$ denote the trajectories discussed in the text. The various phase transition points along these trajectories are represented by thick dots.

III. RESULTS

According to the classical analysis, along the path $\gamma_y = -\gamma_x - 4$ a first-order quantum phase transition should be found at $(\gamma_x,\gamma_y) = (-2,-2)$, and along the path $\gamma_x = -\gamma_y$ second-order transitions should be found at $(\gamma_x,\gamma_y) = (\pm1,\mp1)$. The distinct character of these transitions can be seen in the behavior of of the ground-state expectation value of J_z/j as a function of γ_x, which is half the difference between the numbers of fermions in the excited state and in the ground state. Hence, $\langle J_z/j\rangle = -1/2$ at the first-order phase transition (see the left panel of Fig. 2) implies that 3/4 of the particles occupy the ground state, while in the second-order case the value $\langle J_z/j\rangle = -1$ in the thermodynamic limit implies that all the particles are accommodated in the ground state in the whole range $\gamma_x \in [-1,1]$ (see the right panel of Fig. 2).

The LMG Hamiltonian commutes with the parity operator, i.e., rotations by π around the z axis. We shall consider initial wave packets constructed as linear combinations of

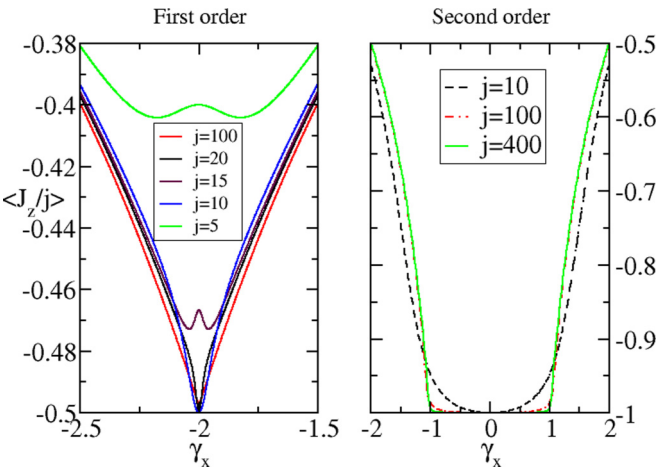

FIG. 2. (Color online) Ground-state expectation value of J_z/j as a function of γ_x. Left panel: 3/4 of the particles occupy the ground state at the transition point in the thermodynamic limit. From top to bottom, the lines correspond to $j = 5$, 10, 15, 20, and 100. Right panel: All the particles are accommodated in the ground state in the whole range $\gamma_x \in [-1,1]$.

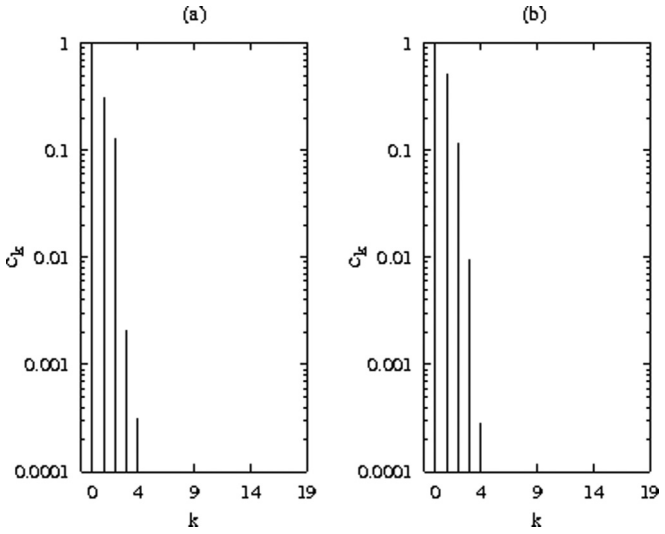

FIG. 3. Gaussian coefficients $c_k = \langle\psi|u_k\rangle$ for a wave packet centered at the ground state and $\sigma = 2$. Left and right panels correspond, respectively, to first- and second-order phase transitions. The k index runs over positive-parity levels only, which depend on the type of transition.

even- (positive-) parity eigenfunctions u_k

$$\psi = \sum_k c_k u_k, \tag{7}$$

with coefficients with Gaussian distributions around the ground state (with label k_0), $c_k \propto \exp[-(k-k_0)^2/2\sigma^2]$, where σ is chosen to include a significant number of energy levels (see below). The time evolution is then given in terms of the eigenenergies E_k by

$$\psi(t) = \sum_k c_k u_k e^{iE_k t}. \tag{8}$$

Experiments where wave packets are constructed in similar form to study quantum revivals are described in, for example, [3,23–25]. In general, revivals are observed when the wave packet is so constructed as to contain a large number of energy levels centered around a highly weighted one. Therefore, very large values of σ could blur the revivals or even prevent them from being observed. On the other hand, taking derivatives over the level index k can be meaningless for a too low σ. The precise values of σ for which the phenomenon is best seen depend, of course, on the particular nature of the system. In Fig. 3 we display the weights of the energy levels used in the construction of the wave packets for both first- and second-order phase transitions. Notice that only positive-parity energy levels are included.

For the sake of illustration, Fig. 4 shows the time evolution of the squared modulus of the autocorrelation function $A(t) = \langle\psi(0)|\psi(t)\rangle$, which is the overlap between the initial and the time-evolving wave packets. This particular case corresponds to the choice $\gamma_x = 0, \gamma_y = 1$, $j = 100$, and $\sigma = 2$. The figure reflects that the wave packet evolves periodically in time in that $|A(t)|^2$ decreases to rather low values (the collapsed state) and returns to its initial value of unity. At early times (see the top panel of Fig. 4), the periodicity corresponds to the classical

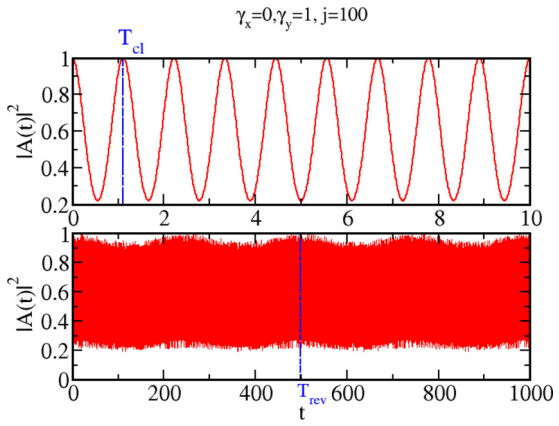

FIG. 4. (Color online) Squared modulus of the autocorrelation function for the early time evolution (top panel) of an initial Gaussian wave packet centered around the ground state. The bottom panel displays the long-time evolution of the same initial wave packet. The vertical, dashed blue lines stand for the classical and revival times as computed through their analytical expressions. (Atomic units.)

one, and in the long run to quantum revivals (the bottom panel of Fig. 4). For consistency, we have verified that both the classical and the revival times obtained from the numerical evolution match those of the analytical expressions $T_{\rm cl} = 2\pi/|E_0'| \approx 1.11$ and $T_{\rm rev} = 4\pi/|E_0''| \approx 499$, the derivatives being simply computed through their numerical approximations $E_0' = E_1 - E_0$ and $E_0'' = E_0 - 2E_1 + E_2$. These are denoted in the figure by vertical, dashed blue lines. The whole picture is better appreciated in Fig. 5, which shows plots of the autocorrelation function for time evolution along a range of trajectories, $\gamma_y = -\gamma_x - 4$ in the top panel and $\gamma_y = -\gamma_x$ in the bottom one. Vertical cuts at constant values of γ_x display a sequence of color-coded collapses (dark regions) and revivals (light regions). Special attention must be paid to the transition points $\gamma_x = -2$ (top panel) and $\gamma_x = \pm 1$ (bottom panel), corresponding respectively to first- and second-order phase transitions, where interestingly the time interval between consecutive revivals increases significantly. The revival times, and the classical times too, actually diverge at the transition points. In the following, we clarify how and why this happens.

First, we focus on the classical time $T_{\rm cl}$, which coincides to a very good approximation with the inverse of the gap. We find that in either case, whether first or second order, as γ_x approaches the transition points $T_{\rm cl}$ grows monotonically up to a finite maximum and that true divergences occur only when $j \to \infty$. Within the numerical precision, the maximum is located right at $\gamma_x = -2$ for the first-order case (see the left panel of Fig. 6). In contrast, the locus of the transition points varies with j for the second-order case but approaches the theoretical values $\gamma_x = \pm 1$ as $j \to \infty$ (the right panel of Fig. 6). Away from the transition points, $T_{\rm cl}$ does not scale with the system size. However, as shown in Fig. 7, right at the transition points the maxima of $T_{\rm cl}$ scale with j, the precise value of the scaling exponents depending on the nature of the transition, namely, $T_{\rm cl} \sim j$ in the first-order case while $T_{\rm cl} \sim j^{0.35(3)}$ in the second.

The classical times also exhibit scaling behavior upon approaching the transition points at fixed j. This is illustrated

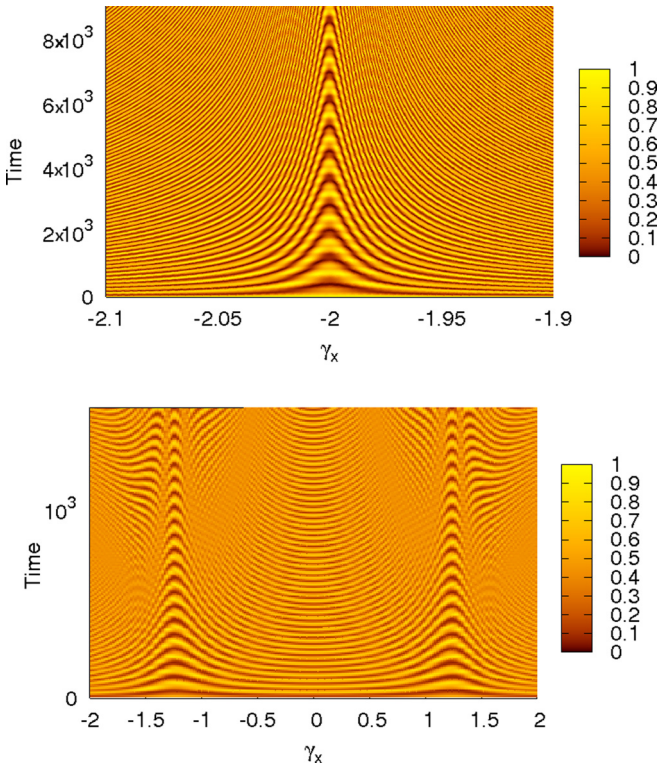

FIG. 5. (Color online) Plots of the autocorrelation function for the time evolution of a Gaussian wave packet centered around the ground state. Dark and light regions correspond, respectively, to collapses and regenerations. The top (bottom) panel is for the first-order (second-order) phase transition. (Atomic units.)

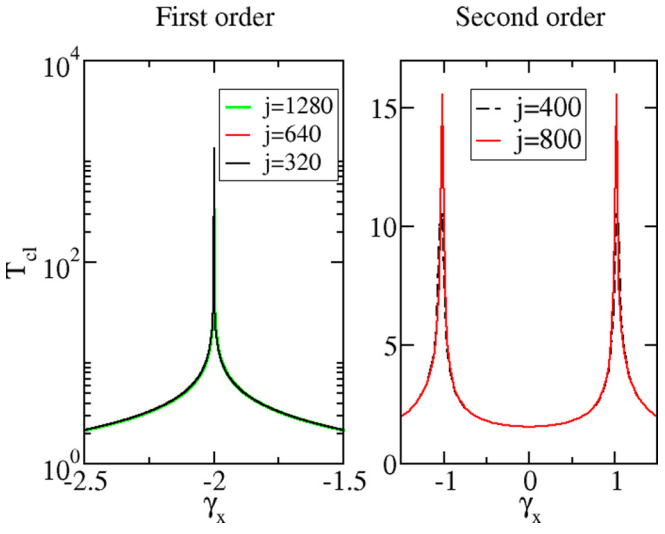

FIG. 6. (Color online) Classical time vs. γ_x. Left panel: Within the numerical precision, the maximum is located right at $\gamma_x = -2$ for the first-order phase transition. Notice the logarithmic scale on the vertical axis. Right panel: The maxima are located near the predicted points ± 1 for second order phase transitions. In either case, first- or second-order, classical times do not scale with j except at the transition points. This is exemplified here for $j = 400$ and $j = 800$. (Atomic units.)

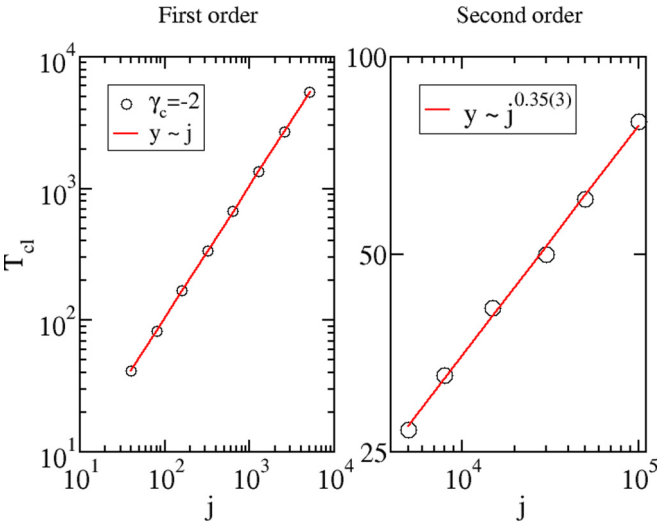

FIG. 7. (Color online) The maxima of T_{cl} scale with j at the transition points, with scaling exponents depending on the type of phase transition: $T_{cl} \sim j$ for the first-order transition (left panel) and $T_{cl} \sim j^{0.35(3)}$ for the second (right panel). The red solid lines are straight-line fits to the data. (Atomic units.)

in Fig. 8, where the left panel corresponds to the first-order phase transition in which case $T_{cl} \sim |\gamma_x - \gamma_c|^{0.51(1)}$, whereas the right panel is for the second-order phase transition and $T_{cl} \sim |\gamma_x - \gamma_c|^{0.50(1)}$. This latter case corresponds to $W = 0$ in Eq. (3) for which a sizable number of analytic results exists. For instance, from the theoretical prediction for the gap around E_{k_c}, $\Delta E = 2\pi\sqrt{\lambda^2 - 1}/\ln N$ if $\lambda > 0$ and $\Delta E \sim N^{-1/3}$ if $\lambda = 1$ [26]. Since the relation between λ and γ_x is $\lambda = 2j/(2j-1)\gamma_x = \gamma_x + O(j^{-1})$ and recalling that $N = 2j$, $T_{cl} \sim |\gamma_x - \gamma_c|^{-1/2}$ and $T_{cl} \sim j^{1/3}$ follow, which are in perfect agreement with our results.

We now turn our attention to the behavior of the revival times. In contrast to T_{cl}, T_{rev} scales linearly with the system

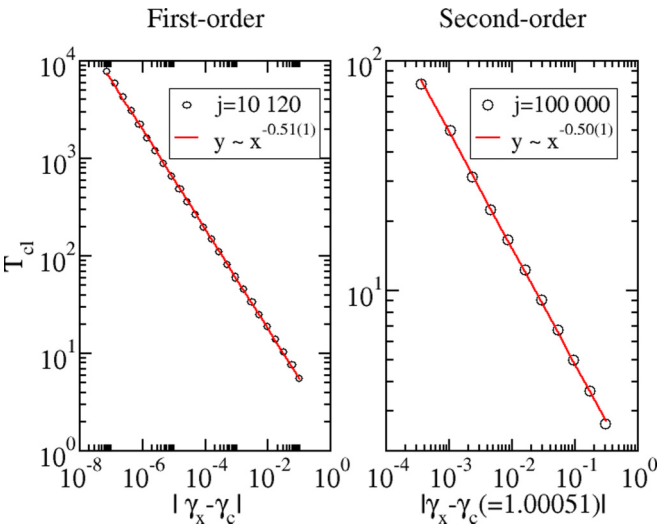

FIG. 8. (Color online) At fixed j, T_{cl} scales with the distance to the transition point as $|\gamma_x - \gamma_c|^{-1/2}$ for both first- and second-order transitions alike. (Atomic units.)

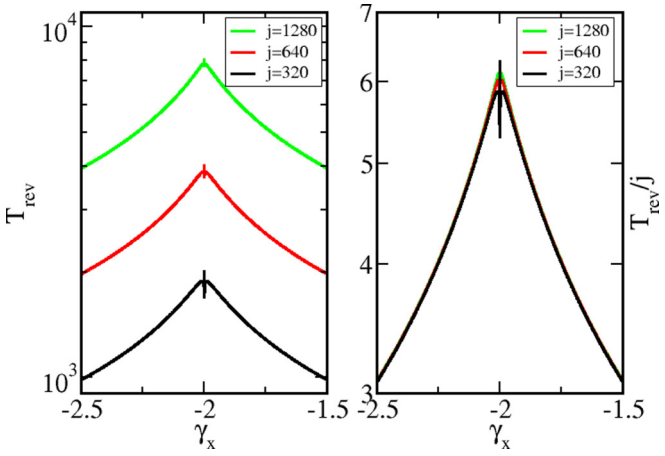

FIG. 9. (Color online) $T_{\rm rev}$ as a function of γ_x for the first-order phase transition. In the right panel, except at the transition point, the data collapse onto a single curve after normalization by the associated system size j. From top to bottom, the lines correspond to $j = 1280$, 640, and 320. (Atomic units.)

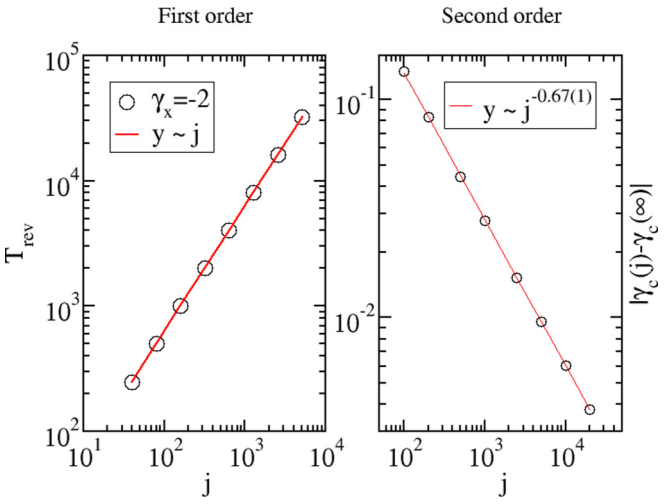

FIG. 11. (Color online) Left panel: Finite maxima of $T_{\rm rev}$ at $\gamma_x = -2$ as functions of j for the first-order phase transition. Right panel: Finite-size corrections to the location of the transition points for the second-order phase transition. (Atomic units.)

size away from the transition points for both the first-order (Fig. 9) and the second-order (Fig. 10) cases. The divergence at $\gamma_x = 0$ in this latter case stems from the equidistant pattern of the energy spectrum for this precise parameter value and is not related to the phase transitions.

Interestingly, but not surprisingly, at the transition points $T_{\rm rev}$ behaves differently in the first- and second-order cases: At the first-order phase transition, $T_{\rm rev}$ shows a finite maximum at $\gamma_x = -2$ for any j. These maxima grow linearly with the system size and there are no signatures of scaling behavior of $T_{\rm rev}$ as a function of γ_x at fixed j. On the contrary, at the second-order phase transition, for any j there always exists a γ_x, closer to $\gamma_c = \pm 1$ for larger j, such that $T_{\rm rev}$ diverges; this will be called $\gamma_c(j)$. The value of γ_x at which $T_{\rm rev}$ diverges scales with the system size as $|\gamma_c(j) - \gamma_c(\infty)| \sim j^{-2/3}$ (Fig. 11). Likewise, at fixed j and on approaching the transition points, $T_{\rm rev} \sim |\gamma_x - \gamma_c|^{-1}$, as depicted in Fig. 12. This peculiar behavior of $T_{\rm R}$ diverging at finite system size is not new as it has been reported previously in the Dicke model of super-radiance and a model for the bending of molecules [5]. Nonanalyticities can be present in finite systems at zero temperature. In this regard, quantum phase transitions without thermodynamic limits have been investigated in [27]. See [28] in the context of Bose gases.

To try to rationalize these findings, consider a wave packet of width $\Delta H = \sqrt{\langle H^2\rangle - \langle H\rangle^2}$. Then $\Delta H \Delta t \geqslant \hbar$, where Δt is the shortest possible time scale for a significant evolution of the wave packet [29]. Hence, clearly $T_{\rm rev} > \Delta t \gtrsim 1/\Delta H$, and consequently it transpires that any characteristic time is ultimately constrained by the statistical uncertainty in the energy. Within this model, and due to the compression of levels at the transition points (i.e., the fact that $E_k - E_0$ vanishes

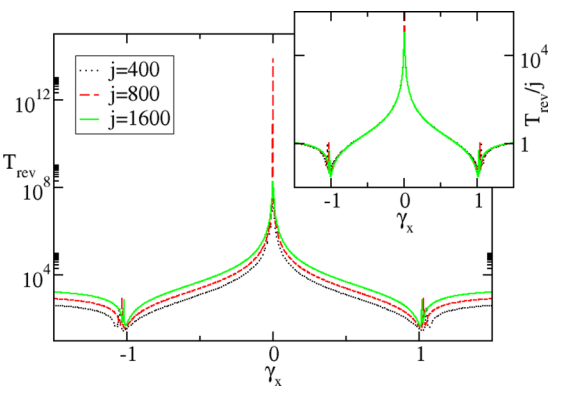

FIG. 10. (Color online) $T_{\rm rev}$ as a function of γ_x for the second-order phase transition. Except at the transition points, the data collapse onto a single curve after normalization by the associated system size j (see inset). The divergences related to the phase transition approach ± 1 as $j \to \infty$. (Atomic units.)

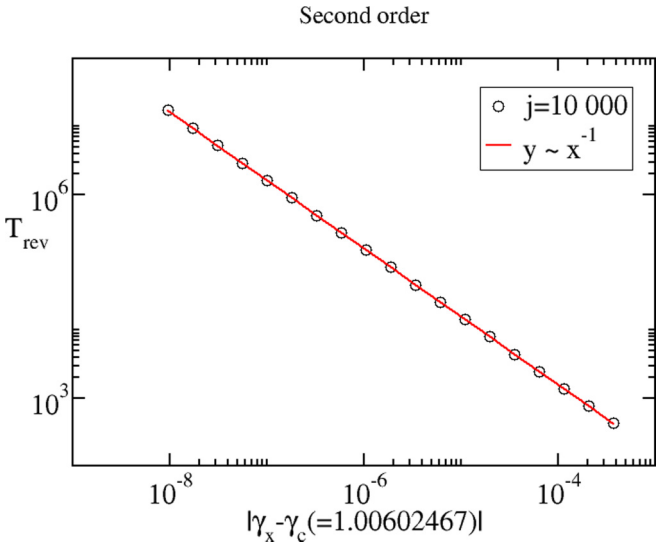

FIG. 12. (Color online) For the second-order phase transition $T_{\rm rev}$ scales with the distance to the value of γ_x at which it diverges. (Atomic units.)

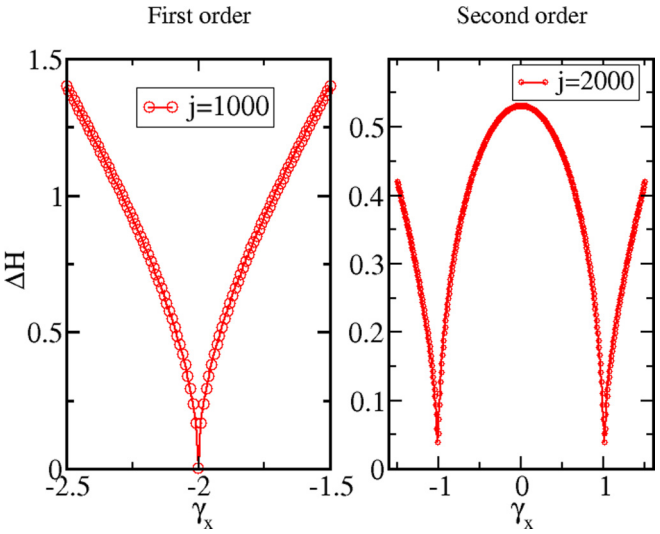

FIG. 13. (Color online) The wave packet; the standard deviation of the energy drops to almost zero as the transition points are approached. (Atomic units.)

upon approaching the transition point or, equivalently, the number of levels within a given energy interval increases), $\Delta H \to 0$, whereby $T_{\rm rev}, T_{\rm cl} \to \infty$, which is in accordance with the findings reported here and with previous results [5]. This fact is a reflection of the well-known occurrence of *slowing down* of the dynamics near critical points.

We have analyzed the behavior of ΔH as a function of γ_x for a state constructed as a linear combination of eigenstates with Gaussian weights $\exp[-(k-k_0)^2/2\sigma]$, and centered around the ground state. We take $\sigma = 1$. At the theoretical (first-order) transition point $\gamma_x = -2$, the variance drops down to almost zero (see the left panel of Fig. 13). There are no finite-size corrections to the location of the critical point nor to the absolute minimum value, which is of order 10^{-4}. Interestingly, ΔH exhibits scaling behavior as $\gamma_x = -2$ is approached, with an exponent value very close to 1/2 (see Fig. 14), which is to

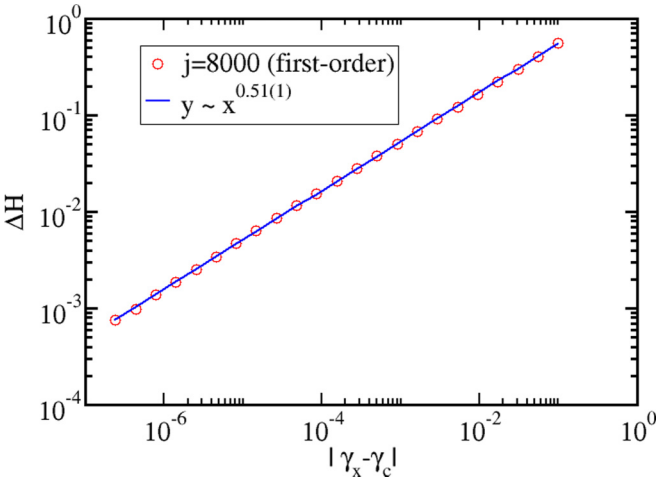

FIG. 14. (Color online) For the first-order phase transition, ΔH decays as a power law with the distance to the transition point $\gamma_c = -2$ with an exponent 1/2. (Atomic units.)

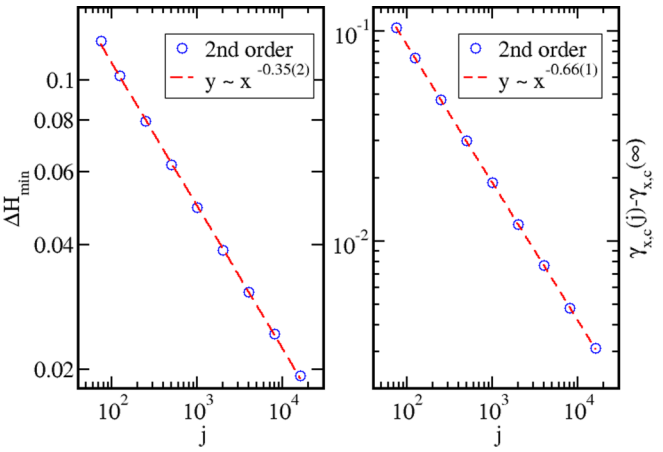

FIG. 15. (Color online) Left panel: Minimum of ΔH as a function of j for the second-order phase transition. Right panel: Finite-size correction to the location of the minimum of ΔH as a function of j. (Atomic units.)

be compared with $-0.51(1)$ and $-0.50(1)$ corresponding to, respectively, $T_{\rm cl}$ and $T_{\rm rev}$ (see Fig. 8). (Notice the trivial change of sign.) A similar behavior is found for the second-order case, the path $\gamma_y = -\gamma_x$, with minima of ΔH vanishing as $\gamma_x \to \pm 1$ (the right panel of Fig. 13). However, in contrast to the first-order case, finite-size effects are evident in Fig. 15 as now $\Delta H_{\rm min} \sim j^{-0.352}$ [to be compared with 0.35(3); see Fig. 7] and, denoting by $\gamma_{x,c}(j)$ the value of γ_x at the minimum ΔH for a given j, $\gamma_{x,c}(j) - \gamma_{x,c}(j=\infty) \sim j^{-0.66(1)}$ [to be compared with $-0.67(1)$; see Fig. 11].

Since ΔH decreases in the thermodynamic limit, a classical analysis may cast light on this issue. The energy surface is the expectation value of the Hamiltonian with respect to the spin-coherent state. It can be interpreted as a Hamiltonian function dependent on variables (θ,ϕ) or, equivalently, the canonically conjugated variables $(\cos\theta,\phi)$ and parameters (γ_x,γ_y). The phase diagram shown in Fig. 1, can be obtained by analyzing the system's fixed points, that is, the points where the the Hamilton equations equal zero. From the classical point of view, this implies that at the transition points of Fig. 1 the system does not move and hence remains stationary. Additionally, it takes an infinite time to reach the transition points, because the closer the system is to them, the more slowly it evolves. This is perhaps the reason that quantum mechanically the mean square standard deviation of the energy for the wave packet tends to zero in both cases when j is large enough. Moreover, the density of levels at those points grows as a function of the size of the system, as can be immediately seen by plotting the energy spectra for any value of j.

Finally, we have compared the several critical exponents obtained for the LMG model in this work and the critical exponents studied in [5] for the second-order quantum phase transition (QPT) in the vibron U(3) and the Dicke models. The results are gathered in Table I where the third column shows values for the vibron model. Superscript asterisks indicate that the same exponent value holds for the Dicke model as well. It transpires that the second-order phase transitions of the LMG and vibron models belong to the same universality class, and arguably those of the Dicke model too. On the

TABLE I. Summary of the several critical exponents discussed in the text and those obtained in [5,30] for the second-order quantum phase transition in the vibron model. A superscript asterisk denotes that the same value is obtained for the Dicke model.

Critical exponents	First-order Lipkin	Second-order Lipkin	Second-order models in [5,30]
$T_{\rm cl} \sim j^{\alpha}$	1	1/3	1/3*
$T_{\rm cl} \sim \lvert\gamma_x - \gamma_c\rvert^{\beta}$	−1/2	−1/2	−1/2
$T_{\rm rev} \sim \lvert\gamma_x - \gamma_c\rvert^{\delta}$		−1	−1*
$\lvert\gamma_c(j) - \gamma_c(\infty)\rvert \sim j^{\eta}$		−2/3	−2/3

contrary, the first-order phase transition appears to be in a different universality class, although the differences affect only finite-size-related exponents.

IV. SUMMARY

We have studied quantum revivals of wave packets centered around the fundamental state in the LMG model. The focus was on the the implications of traversing quantum phase transitions and on how the varied nature of these could affect revival behavior. Far from the transition points our results are qualitatively similar to those of the vibron and the Dicke models, namely, the classical period and the revival time exhibit a smooth nonsingular behavior, and revival times are proportional to the system size. Upon approaching a quantum critical point, however, qualitative differences are observed in the behavior of $T_{\rm rev}$ between first- and second-order phase transitions. $T_{\rm cl}$ diverges as a power law with characteristic scaling exponents in any case. The classical period is found to behave as the inverse of the gap almost perfectly, which shows that our simple, finite approximation to the derivative, $E_n' \approx E_1 - E_0$, leads to correct results. This accuracy is beyond what could be expected, given that our wave packets are not centered around a large quantum number, nor do they comprise a large number of states, which are the assumptions that justify the Taylor expansion performed in Eq. (1). The same is true for $E_n'' \approx E_0 - 2E_1 + E_2$ as shown in the bottom panel of Fig. 4.

At the first-order phase transition, $T_{\rm rev}$ shows finite maxima at $\gamma_x = -2$ that grow linearly with the system size, and no signatures of scaling behavior as a function of the distance $\gamma_x - \gamma_c$. At the second-order phase transition, some traits of the usual scaling behavior are observed while others are not. For instance, as in the vibron and Dicke models, $T_{\rm rev}$ diverges on approaching the transition point even at finite j, in contrast to the usual scenario where divergences develop only as the thermodynamic limit is reached. On the other hand, the loci of these divergences approach their predicted asymptotic limits ± 1 as j increases. This divergent behavior is in accordance with the critical slowing down expected at criticality, and it also agrees with an energy-time, variance-based analysis that can be justified on classical grounds. Finally, as far as only the second-order phase transitions are concerned, a quick glance at Table I reveals that the similarities between the LMG and the vibron models go beyond a comparable qualitative behavior. It can be safely stated that both models belong to the same universality class. However, the finite-size-related exponents are different for each type of QPT (first and second order). It will be interesting to study these properties in other quantum systems to see to what extent these results are universal.

ACKNOWLEDGMENTS

This work was supported by the Projects No. MICINN FIS2009-08451, No. P12.FQM1861 (Junta de Andalucía), CEI-BIOTIC Granada PV8, No. MICINN FIS2011-24149, and CONACyT Project No. 238494.

[1] E. Romera and F. de los Santos, Phys. Rev. B **80**, 165416 (2009).
[2] E. Romera, Phys. Rev. A **84**, 052102 (2011).
[3] R. W. Robinett, Phys. Rep. **392**, 1 (2004).
[4] S. Sachdev, *Quantum Phase Transitions* (Cambridge University Press, New York, 1999).
[5] F. de los Santos and E. Romera, Phys. Rev. A **87**, 013424 (2013).
[6] H. J. Lipkin, N. Meshkov, and A. J. Glick, Nucl. Phys. **62**, 188 (1965); N. Meshkov, A. J. Glick, and H. J. Lipkin, *ibid.* **62**, 199 (1965); A. J. Glick, H. J. Lipkin, and N. Meshkov, *ibid.* **62**, 211 (1965).
[7] O. Castaños, R. López-Peña, J. G. Hirsch, and E. López-Moreno, Phys. Rev. B **74**, 104118 (2006).
[8] P. Ring and P. Schuck, *The Nuclear Many-Body Problem* (Springer, New York, 1980).
[9] M. Kitagawa and M. Ueda, Phys. Rev. A **47**, 5138 (1993).
[10] S. Dusuel and J. Vidal, Phys. Rev. Lett. **93**, 237204 (2004).
[11] G. J. Milburn, J. Corney, E. M. Wright, and D. F. Walls, Phys. Rev. A **55**, 4318 (1997).
[12] A. J. Leggett, Rev. Mod. Phys. **73**, 307 (2001).
[13] A. Micheli, D. Jaksch, J. I. Cirac, and P. Zoller, Phys. Rev. A **67**, 013607 (2003).
[14] C. Pérez-Campos *et al.*, Ann. Phys. (NY) **325**, 325 (2010).
[15] R. Gilmore, *Catastrophe Theory for Scientists and Engineers* (Wiley, New York, 1981).
[16] P. Pérez-Fernández, A. Relaño, J. M. Arias, P. Cejnar, J. Dukelsky, and J. E. García-Ramos, Phys. Rev. E **83**, 046208 (2011).
[17] T. J. Osborne and M. A. Nielsen, Phys. Rev. A **66**, 032110 (2002).
[18] E. Romera, M. Calixto, and Á. Nagy, Europhys. Lett. **97**, 20011 (2012).
[19] P. Zanardi and N. Paunkovic, Phys. Rev. E **74**, 031123 (2006).
[20] S.-J. Gu, Int. J. Mod. Phys. B **24**, 4371 (2010).
[21] O. Castaños *et al.*, J. Phys.: Conf. Ser. **387**, 012021 (2012).
[22] E. Romera, M. Calixto, and O. Castaños, Phys. Scr. **89**, 095103 (2014).
[23] R. A. L. Smith, J. R. R. Verlet, and H. H. Fielding, Phys. Chem. Chem. Phys. **5**, 3567 (2003).

[24] F. Rosca-Pruna and M. J. J. Vrakking, J. Chem. Phys. **116**, 6567 (2002).
[25] S. Will, T. Best, U. Schneider, L. Hackermüller, D. S. Lühmann, and I. Bloch, Nature (London) **465**, 197 (2010).
[26] F. Leyvraz and W. D. Heiss, Phys. Rev. Lett. **95**, 050402 (2005).
[27] D. C. Brody, D. W. Hook, and L. P. Hughston, Proc. R. Soc. London, Ser. A **463**, 2021 (2007).
[28] H.-y. Tang and Y.-l. Ma, Phys. Rev. E **83**, 061135 (2011).
[29] A. Galindo and P. Pascual, *Quantum Mechanics I* (Springer-Verlag, Berlin, 1990).
[30] F. Pérez-Bernal and F. Iachello, Phys. Rev. A **77**, 032115 (2008).